Lagrange: A Three-dimensional Analytic Lens Design Method for Spectacles Application

by

Yang Lu

A thesis
presented to the University of Waterloo
in fulfillment of the
thesis requirement for the degree of
Master of Science
in
Vision Science

Waterloo, Ontario, Canada, 2013

AUTHOR'S DECLARATION

I hereby declare that I am the sole author of this thesis. This is a true copy of the thesis, including any required final revisions, as accepted by my examiners.

I understand that my thesis may be made electronically available to the public.

Abstract

Traditional optical design is a numerical process based on ray tracing theory. The traditional method has the limitation of the application of the spectacle lens because of the necessity of initial configurations and the evaluations of the aberrations of the lens. This study is an initial attempt to investigate an analytic lens design method, Lagrange, which has a potential application in modern spectacle lens for eliminating the limitation of the traditional method.

The Lagrange method can derive the differential equations of an optical system in term of the output and input of the system. The generalized Snell's law in three-dimensional space and the normal of a refracting surface in fundamental differential geometry are used to complete the derivation. Based on the Lagrange method, the solution of a refracting surface which can perfectly image a point at infinity is obtained. Then, a Plano-convex lens and a Bi-convex lens from this solution are designed. In spherical coordinates, the differential equation of the single surface system is:

$$\begin{cases} (-n_2 + n_1 \cos\theta)\,\frac{\partial f}{\partial \theta} - n_1 \sin\theta\, f = 0 \\ \frac{\partial f}{\partial \varphi} = 0 \end{cases} ;\ f(0) = r$$

where f represents the surface. n_1 and n_2 are indices. r is the distance from the vertex point of the surface to the image point. The solution of the equations is:

$$f = \frac{(n_1 - n_2)\, r}{-n_2 + n_1 \cos\theta}$$

In conclusion, the Lagrange solves unknown lens surface based on definable inputs and outputs according to customer requirements. The method has the potential applicants of the modern customized lens design. Moreover, the definable outputs make the simultaneous elimination of several aberrations possible.

Acknowledgements

I would like to acknowledge my supervisor Dr. Vasudevan Lakshminarayanan who gave me the opportunity to be a master's student. Your patient guides and smart instructions help me lead to the completion of this thesis. I also would like to thank to Dr. Hart Katz, who taught me a lot of mathematics knowledge which is the foundation of the thesis. I extend my thanks to my committee members, Dr. Simarjeet Saini and Dr. William Bobier, for your remarkable support and concern throughout. Thanks to the members of Dr. Vengu's lab for setting a comfortable working atmosphere and to my friends in School of Optometry who have contributed and assisted on my work. Finally, I would like to thank my parents for your concern and support. I could not have done this without your support.

Table of Contents

List of Figures

List of Tables

Chapter 1
Spectacle Lens Design Review

1.1 Introduction

Spectacle Lenses are used to correct the refractive errors of the eye and hence improve visual acuity and performances. Spectacle lenses are special imaging systems because they are combined with the eye's optics, which increases its complexity. Traditional design methods use the simplified eye model, which only contributes an optical aperture of the whole system. This chapter summarizes the basic principles of the traditional spectacle lens, and briefly introduces current trends of modern spectacle lens design.

1.2 Fundamental Concepts for Traditional Spectacle Lens Design

1.2.1 Far Point and Far Point Sphere

The far point is the on-axis point which is conjugate with its image on retina (fovea vision) when the eye is not accommodating. Figure 1.1 illustrates the far points for the emmetropic, myopic and hyperopic eye. The far point for emmetropic eye is at infinity. For myopic eye, it is in front of the retina, and for hyperopic eye, it is behind the retina.

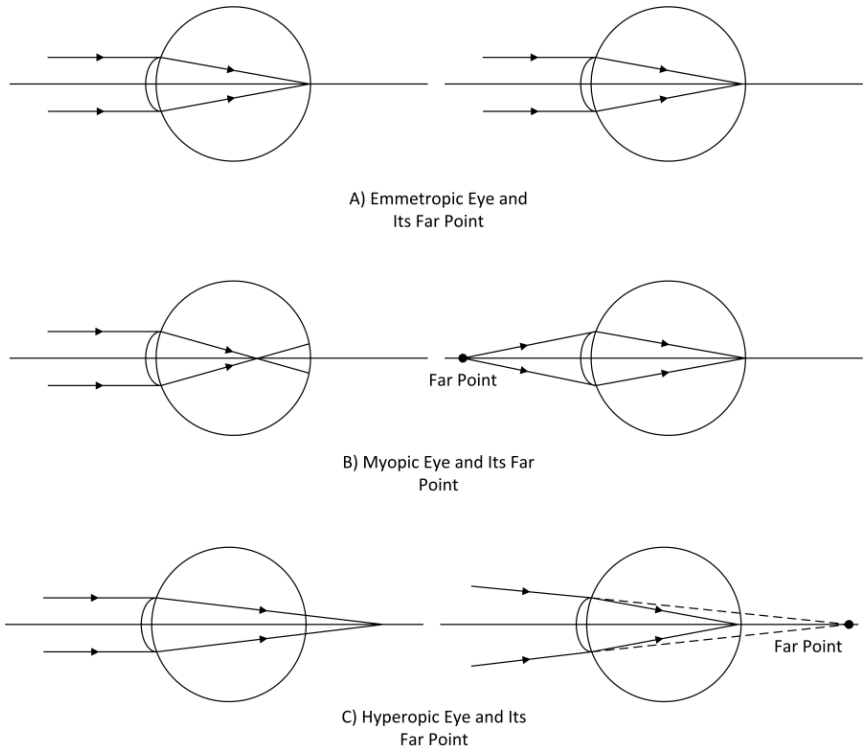

Figure 1.1 The definition of the far point

When the eye rotates, the far point will follow the rotation. As a result, a far point sphere is formed in a three dimensional space. The center of the far point sphere is same as the center of the eye rotation. Figure 1.2 illustrates the spectacle lens corrections for a hyperopic eye and a myopic eye respectively. The axis of symmetry of the lens is the lens optical axis. Because of the eye rotation, an object sphere is also made. Traditional spectacle lens design assumes that the stop size of the system is infinitesimally small, and the effective stop is at the center of the eye rotation[1]. The eye rotation increases the complexity of the spectacle lens and makes the system dynamic.

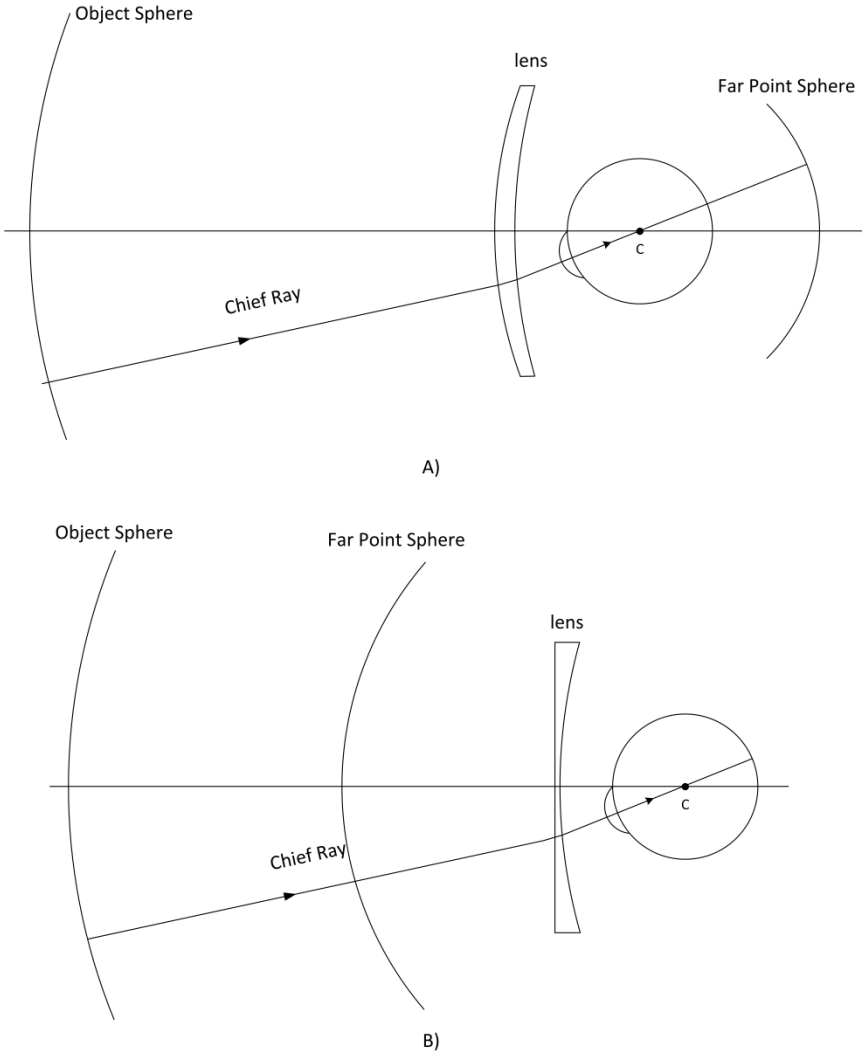

Figure 1.2 The far point sphere: A) the correction for a hyperopic eye B) the correction for a myopic eye

1.2.2 A Perfect Imaging System and Spherical Spectacle Lens Aberration

Figure 1.3 shows a perfect imaging system, and only chief rays are drawn here[2]. C is the center of the entrance pupil. All the lights coming from the edges of the object, P and Q, will be focused at the edges of the image, P' and Q' respectively. The lights from an arbitrary point on the object, O, will be focused on the image point, O'. The distance OZ and O'Z' has the relation: OZ=m*O'Z', where m (a constant) is the magnification of the system. Theoretically, an infinite number of surfaces (degrees of

freedom) are needed to perfectly image infinite number of points[2]. A spectacle lens only has two surfaces, which also increases the design difficulty.

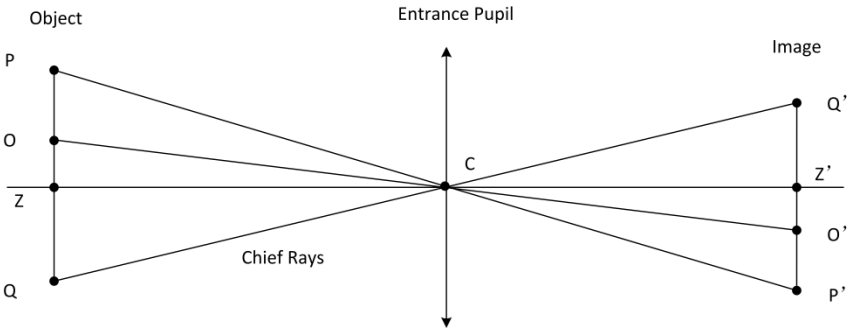

Figure 1.3 A perfect imaging system

Traditional spectacle lenses use spherical surfaces. A spherical surface can image a point, but suffers from aberrations. Aberration is defined as the deviations of the rays from the ideal image on the image plane[3]. Aberrations are categorized into chromatic aberrations and monochromatic aberrations. Chromatic aberrations are dependent on the material and hence the refractive index of the lens, and will not be discussed here. Ray tracing methods are used to calculate monochromatic aberrations. The paraxial image (Gaussian image) is considered as the ideal image. Aberrations can be expressed as a power series with different orders[4].

Only third order aberrations are considered in the spectacle lens design. They are spherical aberration, coma, oblique astigmatism, field curvature and distortion. Practically, the aberrations of a lens system are the combinations of these individual aberrations[5].

It is impossible to correct all these aberrations with two surfaces. According to Atchison, the aberrations greatly relying on pupil size can be neglected for spectacle lens system[1]. Therefore, both spherical aberrations and comas which are highly dependent on pupil size do not affect the image quality of the eye and spectacle lens system.

Spherical aberration is formed because the paraxial rays and the marginal rays from an on-axis point are not focused at the same point by the lens. As shown in Figure 1.4, the spherical aberration is the difference between the focuses of the paraxial rays and the marginal rays. The formation of coma has the similar reason as the spherical aberration formation. The difference is whether the object is on the optical axis or not. Figure 1.5 illustrates the coma of a lens. The paraxial rays are focused as a point on the image plane, whereas the marginal rays are imaged as a circle. Both the spherical aberration and coma can be drastically reduced by adding a small pupil to reduce the marginal rays.

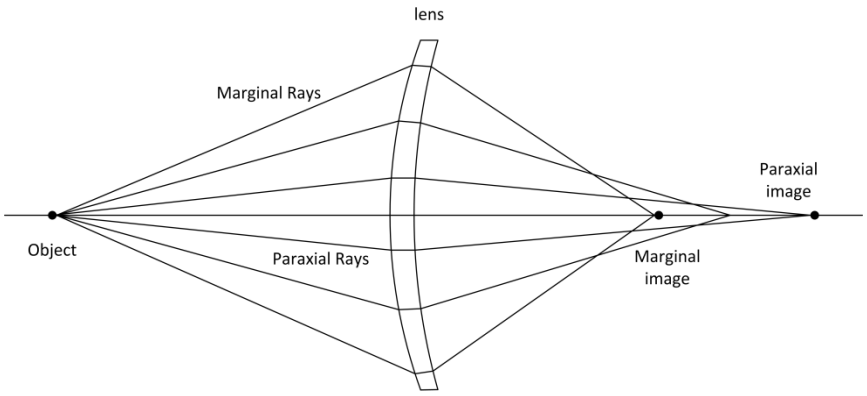

Figure 1.4 The spherical aberration of a plus spherical lens

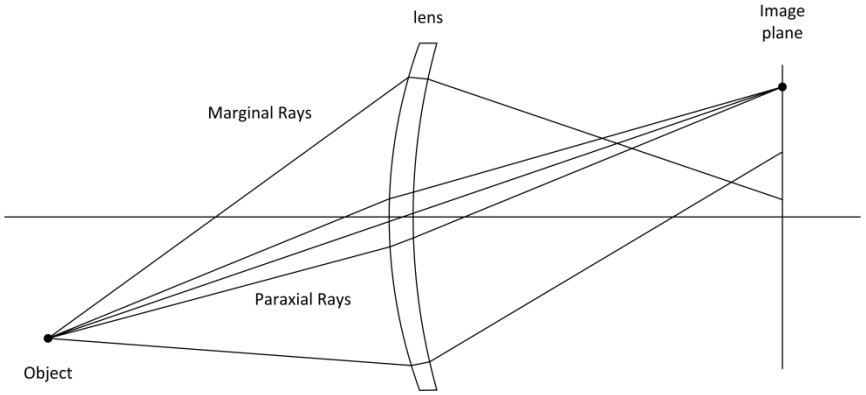

Figure 1.5 The coma aberration of a plus spherical lens

The correction of oblique astigmatism is a major objective for the spectacle lens design. Oblique astigmatism is produced when a pencil of light from an off-axis point is refracted obliquely

by a spherical surface[6]. Figure 1.6 and Figure 1.7 illustrate the principle of the oblique astigmatism. In Figure 1.6, only tangential rays are drawn. O is an off-axis point. The lens optical axis is the rotation symmetry axis of the lens surface. C is the curvature center, and the axis passing through OC is known as auxiliary axis. This axis is also the rotation symmetry axis. For this axis, O becomes an on-axis point. The principle ray and the lens optical axis define the tangential plane. The rays in the tangential plane are imaged as a line O_1O_2. The image of the paraxial rays of the principle ray is at somewhere between O_1O_2. In Figure 1.6, it is shown as Ot.

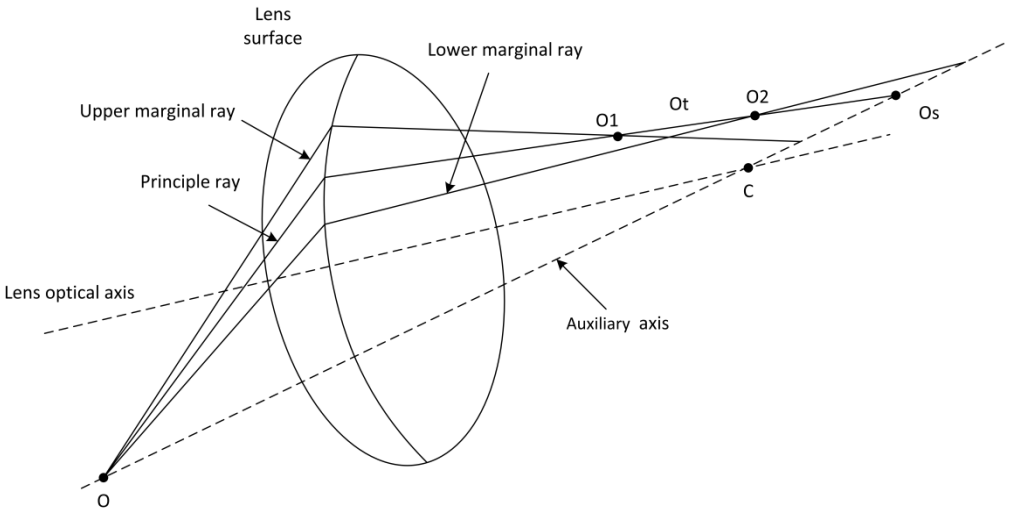

Figure 1.6 Oblique astigmatism: tangential rays only

The sagittal rays are illustrated in Figure 1.7. The sagittal rays and the principle ray all pass through a sagittal circle on the surface. The sagittal circle is rotation symmetric around the auxiliary axis. The sagittal image is on the auxiliary axis because the sagittal rays are rotational symmetric. It is obvious that the sagittal image Os is not coincident with the tangential image Ot, as shown in Figure 1.6.

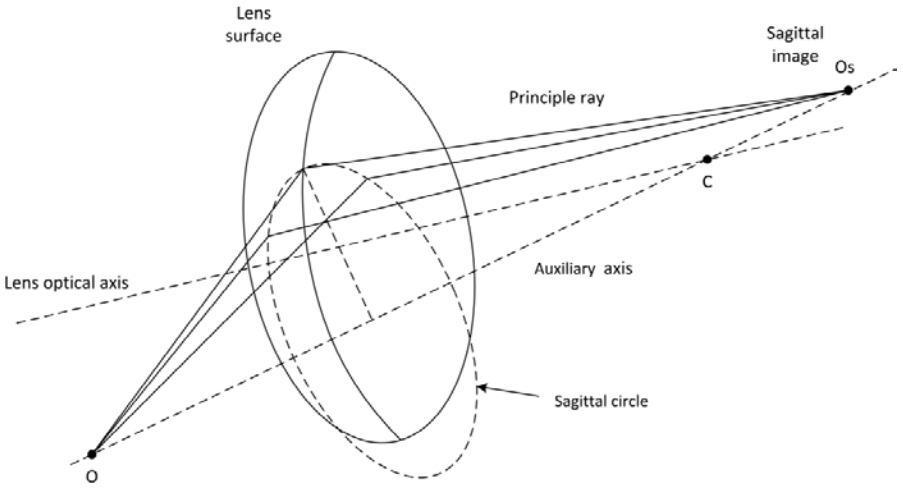

Figure 1.7 Oblique astigmatism: sagittal rays only

For a single spherical surface, the locations of the sagittal and tangential images can be found by Coddington equations[7]. Figure 1.8 illustrates the layout for the tangential focus. O is the object, and Ot is the tangential image. OAOt is the principle ray, and OA'Ot is a paraxial ray. The AA' is so small that it can be regarded as the tangential line which is vertical to the normal CA. -t is the length of OA. The negative sign is added if the object is at the left side of the surface. t' represents the length of AOt. U is the angle between OA and the lens axis. θ is the angle between the normal CA and the lens axis. i is the incidence angle, and i' is the refraction angle. BA is vertical to OA. Then, we have the following relations:

$$\theta = i - U \Leftrightarrow d\theta = di - dU \tag{1-1}$$

In the triangle OAB, we have:

$$AB = -t\,tan\,dU \approx -t\,dU \tag{1-2}$$

In the triangle AA'B, because AA' is vertical to AC and AB is vertical to OA, the angle A'AB is equal to i. Therefore, we have:

$$AB = AA'\,cos\,i \tag{1-3}$$

In the sector ACA', we have:

$$AA' = r\ d\theta \tag{1-4}$$

where r is the radius. Combine all the equations above, we have:

$$AB = -t\ (di - d\theta) = r\ cos\ i\ \ d\theta \tag{1-5}$$

For the refracted ray, we have the similar equation as:

$$-t'\ (di' - d\theta) = r\ cos\ i'\ \ d\theta \tag{1-6}$$

By differentiating the both sides of Snell's law, we have:

$$n\ cos\ i\ \ di = n'\ cos\ i'\ \ di' \tag{1-7}$$

where n and n' are the object space index and the image space index respectively. Combining the equations 1-5, 1-6 and 1-7, we obtain the Coddington equation for the tangential focus:

$$\frac{n'\cos^2 i'}{t'} - \frac{n\cos^2 i}{t} = \frac{n'\cos i' - n\cos i}{r} \tag{1-8}$$

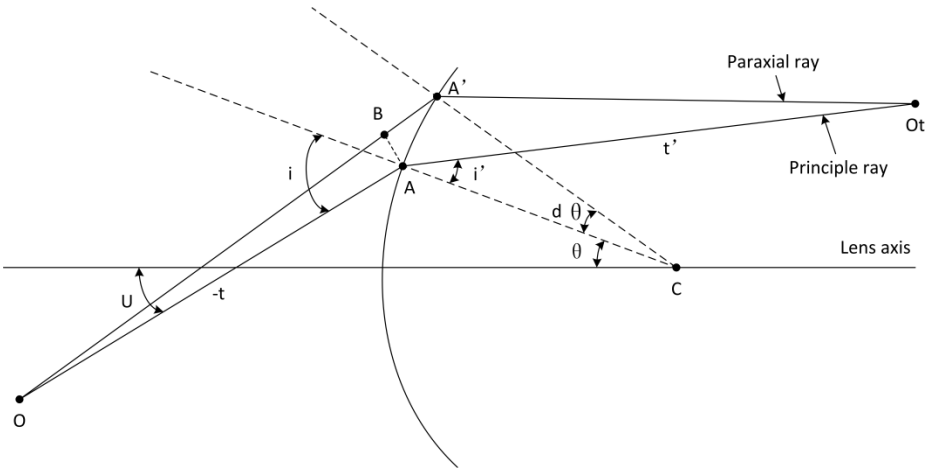

Figure 1.8 The tangential image layout

Now we derive another Coddington equation for the sagittal focus. The layout is shown as Figure 1.9. O is the object and Os is the sagittal image. The ray OAOs is the principle ray. $-s$ is the length of OA. s' is the length of AOs. OC is the auxiliary axis. The sagittal image Os is on the auxiliary axis. Notice that the area of the triangle OAOs is equal to the sum of the areas of the triangle OAC and ACOs. The area of a triangle XYZ is given by $\frac{1}{2}\ XY\ YZ \sin Y$. Therefore, we have:

$$-\frac{1}{2}\, s\, s' \sin(180° - i + i') = -\frac{1}{2}\, s\, r \sin(180° - i) + \frac{1}{2}\, s' r \sin i'$$

$$\Leftrightarrow s\, s' \sin(i - i') = -\, s\, r \sin i + \, s'\, r \sin i'$$

$$\Leftrightarrow -\frac{n' \sin i \cos i' - n' \cos i \sin i'}{r} = -\frac{n' \sin i}{s'} + \frac{n' \sin i'}{s} \tag{1-9}$$

Then, according to Snell's law, $n\, sin\, i = n' \sin i'$, we have the Coddington equation for the sagittal focus as:

$$\frac{n' \cos i' - n \cos i}{r} = \frac{n'}{s'} - \frac{n}{s} \tag{1-10}$$

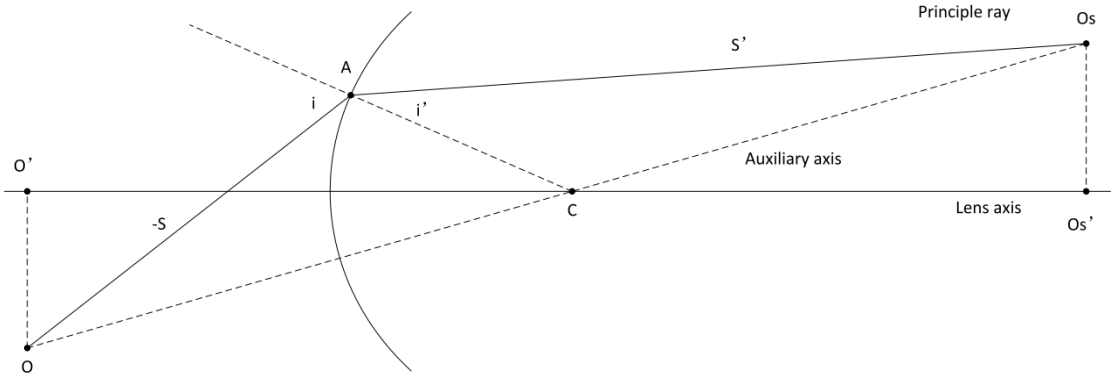

Figure 1.9 The sagittal image layout

In terms of the Coddington equations and the third-order theory, the sagittal and tangential power errors of a thin spectacle lens are given as:

$$Fs' = Fo + F_L + Es \tag{1-11}$$

$$Ft' = Fo + F_L + Et \tag{1-12}$$

where Fs' and Ft' are sagittal and tangential focus vergences. Fo is the object vergence, and F_L is the power of the lens. Es and Et are the sagittal and tangential power errors. We have:

$$Es = y^2\, X = y^2\, \frac{F_L}{n\,(n-1)^2}\left\{{F_2}^2\, \frac{2\,n+1}{2} + F_2\, \frac{-F_L\, n\,(n+2)+2\,l\,(n^2-1)}{2} + \frac{[F_L\, n - l\,(n-1)]^2}{2}\right\} \tag{1-13}$$

$$Et = y^2\, Y = y^2\, \frac{F_L}{n\,(n-1)^2}\left\{{F_2}^2\, \frac{4n+5}{2} + F_2\, \frac{-F_L\,(n-2)^2+2\,(3l+2Fo)\,(n^2-1)}{2} + \frac{{F_L}^2\, n\,(n+2)}{2} - F_L\, l\,(n - 1)(n+2) - F_L\, Fo\, n\,(n^2-1) + \frac{l^2\,(2\,n+1)\,(n-1)^2}{2} + 2\, l\, Fo\,(n-1)(n^2-1)\right\} \tag{1-14}$$

where y is the height of the principle ray. l is the distance from the vertex of the back surface to the center of the rotation of the eye. F_2 is the power of the back surface[8]. Eventually, the oblique astigmatism of the thin spectacle spherical lens is given as:

$$\mathrm{OA} = Et - Es \tag{1-15}$$

Field curvature is discussed when the oblique astigmatism has been corrected. Now, the off-axis point is perfectly imaged in the local paraxial area defined by the chief ray. Field curvature is produced because the images of the objects at infinity lie on a curved surface rather than a plane surface. This curved surface is known as the Petzval surface. The curvature of the Petzval surface is expressed as: $\frac{-F_L}{n}$, where F_L is the power of the lens and n is the index of the lens material[9].

Distortion is evaluated when the field of curvature does not exist. Distortion is produced because the magnification of the spherical lens is not a constant from its center to periphery. There are two kinds of distortion. First, the distortion changes the shape of the image in peripheral vision when the eye looks though the center of the lens. Second, the distortion also occurs when the eye rotates to use the edge of the lens[10]. Figure 1.10 illustrates these two cases.

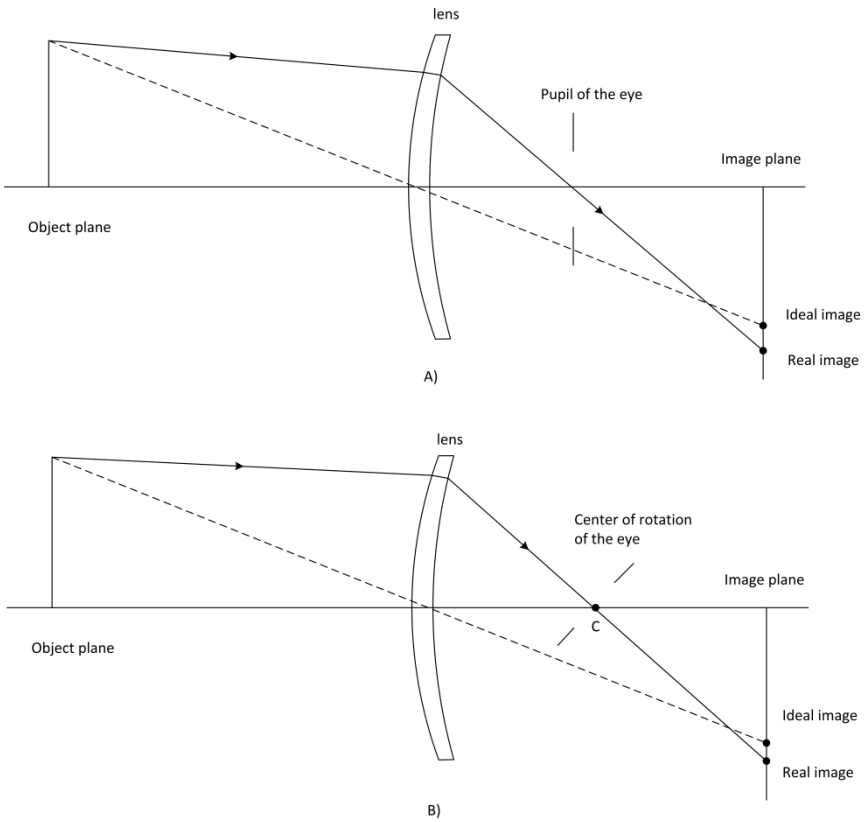

Figure 1.10 Spectacle lens distortion: A) the eye looks straight B) the eye rotates

1.3 Single Focal Spectacle Lenses Principle

Traditional spectacle lens images the distant object onto the far point of the eye to correct the refractive errors, such as myopia, hyperopia and astigmatism. The astigmatic eye has an asymmetric corneal curvature, and the horizontal and vertical curvatures are unequal. As a result, the rays in these two planes are focused at different positions on the optical axis. This leads to a blur image on the retina. Ocular astigmatism is usually combined with myopia or hyperopia. Traditionally, astigmatic eyes can be corrected by sphero-cylindrical, toric and atoric lens. Here, we only discuss the eye without astigmatism for simplicity. Details of the corrections of the astigmatic eyes can be found in Jalie's book, the principles of ophthalmic lenses.[6]

Spectacle lenses have two main categories, single focal lens and multifocal lens. Single focal lens has the same power on the entire lens. It can be designed for either distant vision or near vision in terms of the different requirements of the wearers.

Multifocal lenses are produced for the correction of presbyopia. Presbyopia refers to a condition in which the eye loses accommodation. A multifocal lens is separated into two or three parts which have different powers corresponding to distant, intermediate and near vision. Patients with multifocal lenses suffer from image jump and blind areas because of the sharp boundary between these segments. To solve this problem, progressive addition lenses were invented. The simplest progressive addition lens inserts a corridor zone between the distance and near viewing areas. As shown in figure 1.11, this corridor zone has continuous spherical power change along a vertex line[11]. Minkwitz theorem proofs that the continuous power change will bring unwanted astigmatism whose axis is oblique. The detailed Minkwitz theorem can be found in reference [12]. This unwanted astigmatism will result in a serious swimming effect in the periphery areas of the lens, which becomes huge barrier for the universal use of the progressive lens. The swimming image occurs because the magnification difference in the lens periphery distorts the observed movement of an object from the actual physical movement[11]. This imaging distortion is known as skew distortion. The skew distortions are produced when the axis of the lens astigmatism in each point of the lens periphery are not parallel to the vertical or horizontal plane, i.e. oblique[13]. The correction of this distortion is the main target of the progressive lens designer.

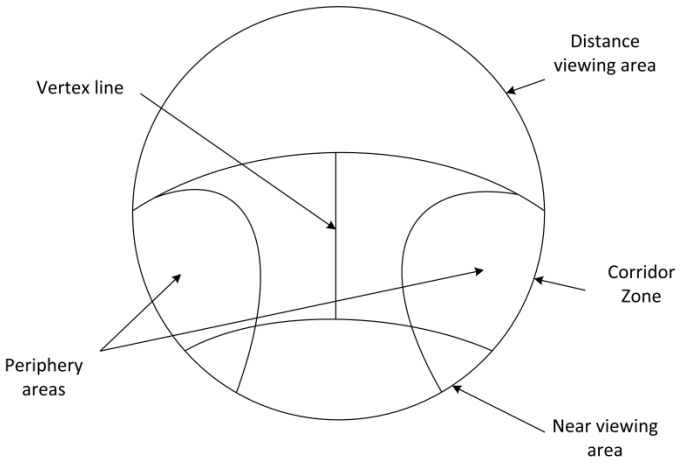

Figure 1.11 A progressive addition lens

There are three methods for the single focal lens design in terms of three different objectives[14]:

1) Eliminating Oblique Astigmatism

Oblique astigmatism is eliminated when the sagittal and tangential focuses are coincident. This target can be achieved by choosing a base curve (usually the front surface) in terms of the Tscherning's ellipse, which was demonstrated by Marius Tscherning in 1904. Figure 1.12 shows the Tscherning's ellipse under the thin lens approximation, and this lens is designed for the distant vision. The top half of the ellipse is the Ostwalt form leading to a flat surface solution, whereas the bottom half of the ellipse is the Wollaston form leading to a steep surface solution. The solution of the Wollaston part is not widely used for spectacle lens because the steep curvature affects the cosmetic appeal of the wearers[15]. The equation of the Tscherning's Ellipse is given as:

$$F_1{}^2\,(n+2) - F_1\left[\frac{2}{l}\,(n^2-1) + F_L\,(n+2)\right] + n\left[F_L + \frac{n-1}{l}\right]^2 = 0 \qquad (1\text{-}1)$$

where, F_1 is the base curve power; n is the index of the lens; F_L is the total power of the lens; l is the distance from the vertex of the back surface to the center of the eye rotation[16]. In Figure 1.12, notice that the range of the lens power is from +7 D to -23.25 D. Out of this range, the oblique

astigmatism can only be minimized. This kind of lens is known as point-focal lens. Detailed third-order equations and the derivations of the Tscherning's ellipse for both the spherical and aspheric lens can be found in references [17][8].

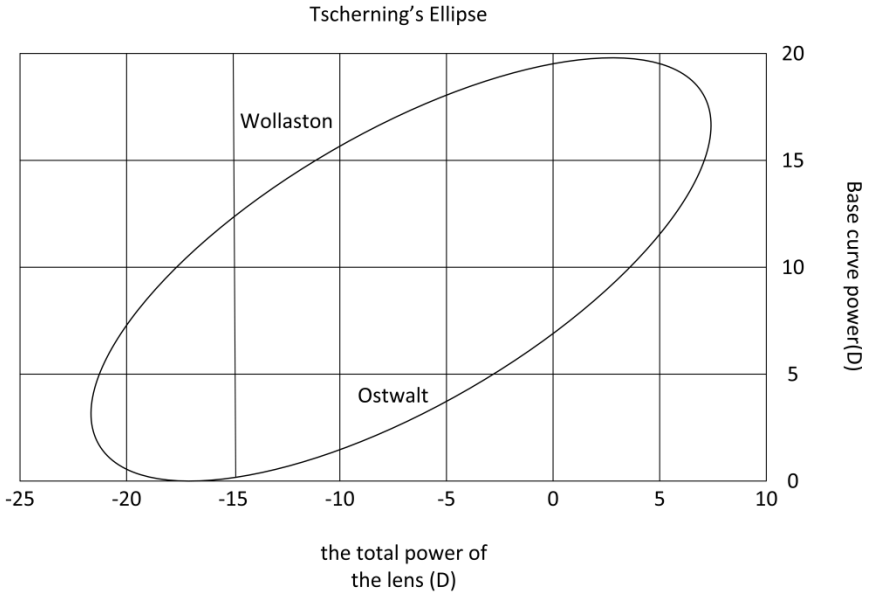

Figure 1.12 Tscherning's ellipse for thin lenses

2) Reducing Mean Oblique Power Error

The point-focal lens can eliminate or minimize oblique astigmatism, but it cannot correct the field of curvature. The image of the point-focal lens is on its Petzval surface rather than the far point sphere, as shown in Figure 1.13. Therefore, the concept of mean oblique power error is introduced. Mean oblique power error is defined as $\frac{Es+Et}{2}$, where Es is the tangential power error, and Et is the sagittal power error. The lens whose mean oblique power error is zero is known as the Percival lens. This lens is bent so that the image of the least confusion is on the retina. The far point sphere is somewhere between the tangential focal shell and the sagittal focal shell, as shown in Figure 1.14. However, the solution of zero mean oblique error is slightly different from the solution of the least confusion[17].

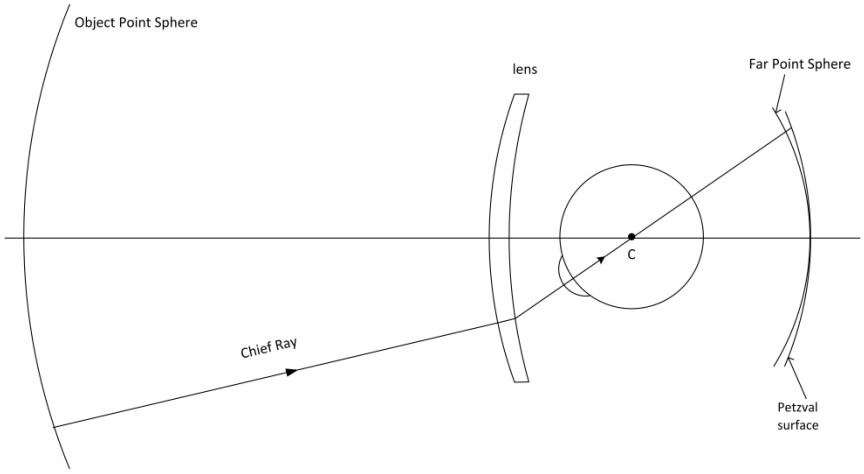

Figure 1.13 The point-focal lens design

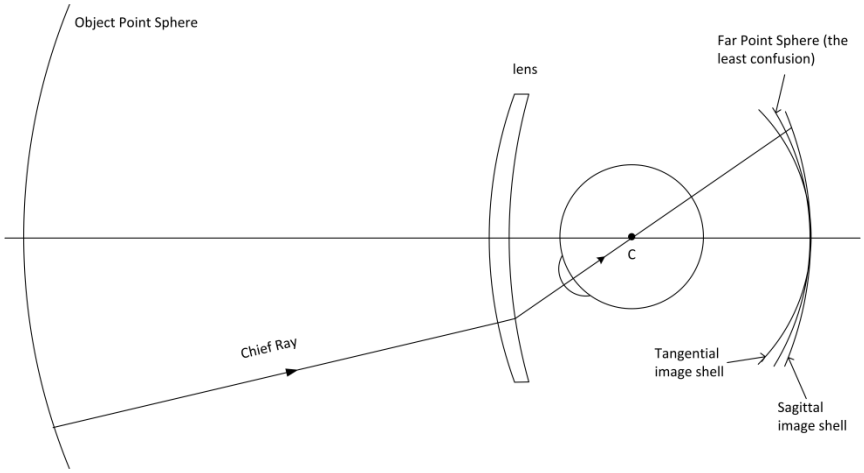

Figure 1.14 The Percival lens design

3) Eliminating Tangential Error

The minimum tangential error lens is designed to let $Et = 0$. The lens is free from the tangential power error. Many commercial lens series use this form to balance the performance of the lens for flexible real vertex distances. The real vertex distance refers to the distance from vertex of the back surface to the center of the eye rotation. When this distance is longer than the empirical distance (usually 27cm), the lens performance is similar to a point-focal lens. On the other hand, the lens performance is similar to a Percival lens[18].

There are two obvious defects for the spherical lens. First, as mentioned above, the power range of the astigmatism free lens is limited from +7 D to -23.25 D. The spherical lenses are not effective, especially for high positive lenses. Second, because of the limited degree of freedom of the spherical lens, the off-axial aberrations cannot be reduced simultaneously[19][20]. Therefore, aspheric lens was invented to overcome these barriers. The aspherical surface can be expressed as:

$$z(r) = \frac{c\,r^2}{1+\sqrt{1-(1+k)c^2\,r^2}} \tag{1-2}$$

where $z(r)$ represents the sag of the surface (the height at each point); r represents the radial distance from the z axis; c represents the curvature at vertex, and k is known as conic constant. If one of the lens surface is aspheric, there are two or three solutions for the back and front surfaces, and both the oblique astigmatism and mean oblique error can be effectively reduced simultaneously[17]. More complicated aspherical surface is expressed as:

$$z(r) = \frac{c\,r^2}{1+\sqrt{1-(1+k)c^2\,r^2}} + \alpha_4\,r^4 + \alpha_6\,r^6 + \alpha_8 r^8 + \cdots \tag{1-3}$$

where α_i is the coefficient of the polynomial. These extended terms increase the surface complexity and the degree of freedom. This makes the elimination of several aberrations achievable. The extended aspheric surface is applied in many lens patents, such as the US patent 4,504,128, US patent 6,012,813, and European patent 0,886,166,B1.

1.4 Modern Lens Design and Current Spectacle Lens Design

In lens manufacturing industry, Lens blanks are categorized as finished and semi-finished lens blanks[21]. Finished lenses have both the front and back surfaces completed, and are ready to be used by an optical dispensary. A combination of the finished lenses can be chosen for the specific power prescription of a patient. However, semi-finished lenses have one of the surfaces unfinished. The semi-finished lenses are mostly used by multifocal lenses. The completed surface usually contains the

base curve and power arrangement. Then, the unfinished surface is cut and polished in terms of the suitable power and axis for the completed surface.

Traditional lens surfaces include spherical, toric and aspherical surfaces, and traditional spectacle lens products are the lens series (finished lenses) rather than customized lenses (semi-finished lenses). Nowadays, the increasing demands of the better vision and various visual requirements of the wearers stimulate the development of the personalized lens, and the more complicated lens surface is required, especially for the multifocal lenses. Fortunately, current technologies can manufacture complex lens surface. Free-form lens surface can be made by advanced computer-aided and ultra-precision surfacing and polishing technologies[22][23]. Mathematically, the free-form surfaces are expressed by either analytic functions, such as polynomials, or exact mathematic expressions. Therefore, new lens design concepts and techniques can potentially provide novel solutions.

In this thesis, an analytic design method called Lagrange will be introduced in chapter 2. The Lagrange provides an analytic lens surface solution which can combine all aberrations. This method can design entire lens area and increase the degree of freedom. Chapter 3 derives the equation and its solution based on a single surface system which can perfectly image a point on optical axis. Chapter 4 discusses two lens design examples in terms of the solution given in chapter 3. Chapter 5 provides the conclusions from the above discussions and the future work.

Chapter 2
Introduction to Lagrange Optical Design

2.1 Background

Traditional optical design is a forward and numerical process. Figure 2.1 illustrates this process. First, the initial configuration of a lens is chosen. Then, the aberrations of the lens are calculated by ray tracing. At last, the lens solution is determined by modifying the lens parameters, such as the surface curvatures and material indices. Modern optical design software, such as Zemax or Code V, can target more than one aberration in terms of sophisticated metric functions, but the initial configurations of the lens are still needed.

This automatic lens design method is known as optimization. Based on this method, a free-form progressive lens designed in Zemax was introduced by Tocci, in 2007.[24] Combining with a complex eye model (Liou and Brennan, 1997), both the front and back surfaces of the lens were optimized to image far, mid-range and near objects in terms of the rotation of the eye model. The back surface was expressed by a polynomial which has 40 terms, and all their coefficients were modified during optimization. After the optimization, the back surface became a free-form surface which leaded to an outstanding performance of the lens corresponding to the far, mid-range and near configurations. The enormous calculations of the aberrations and ray tracing make the optimization a time-consuming task, and the selection of the initial point also restrict its usage within only experienced optical designers.

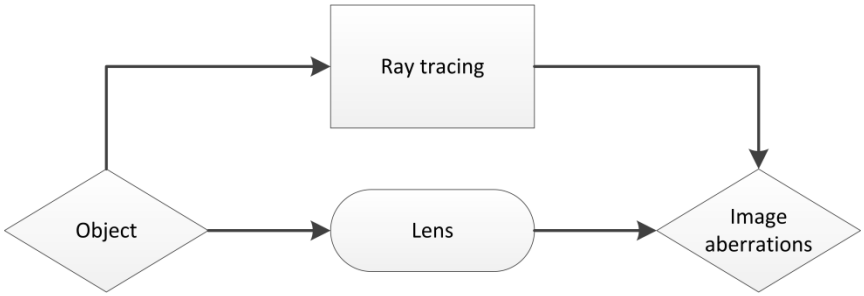

Figure 2.1 The forward optical design process

This chapter introduces an analytic and inverse technique which breaks the barrier of the initial configurations and the aberration calculations. We name this technique Lagrange.

2.2 Lagrange Design Method

Figure 2.2 demonstrates the Lagrange design process. This process can be described as finding an unknown optical system by the given input and output ray fields, which are unified vector functions with the system parameters as variables. The ray tracing is stilled need, but we avoid calculating the aberrations because the output is already given. In this sense, it is an inverse and analytic process. Now, we need to build a relation between the input, the system and the output.

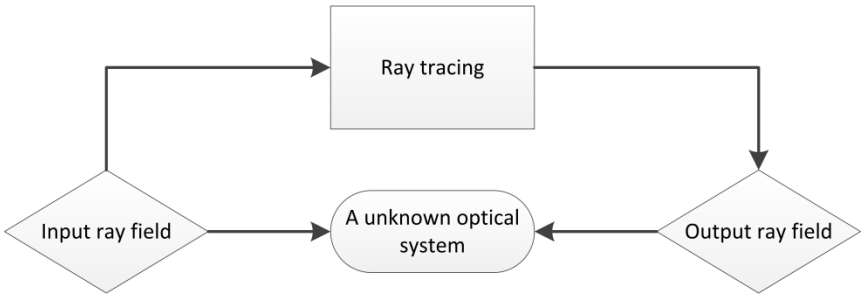

Figure 2.2 The Lagrange design process

Suppose that we have a multi-surface lens system, as shown in Figure 2.3. In the Figure, f_i represents the i th surface. R_i represents the input ray field of the i th surface, and R_{i+1} represents the output ray field. n_i is the index. The input ray field is refracted by each surface, and the output ray field becomes the input of the next surface. In order to solve the surface f_i, we need to find the

mathematical relations among f_i, R_i and R_{i+1}. It is well known that the light propagation between different mediums follows Snell's law. Based on the Snell's law, a system of the equations based on the ray refraction on each surface can be derived. The analytic solutions of the surfaces are obtained by solving the associated equations.

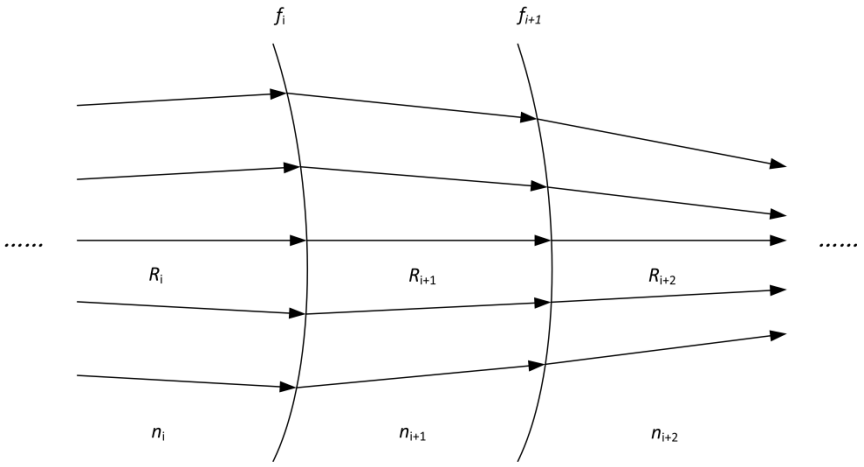

Figure 2.3 A multi-surface optical system

2.3 Snell's Law in Three-dimensional Space and the Surface Normal

In order to find the relation among the input, the output and the surface, Snell's law is needed. In two-dimensional space, it is well-known that Snell's law is expressed as:

$$n_i \, sin\alpha_i = n_{i+1} \, sin\alpha_{i+1} \tag{2-1}$$

where α_i is the incident angle. α_{i+1} is the refracted angle. n_i is the index. However, In three-dimensional space, Snell's law is presented as a vector form which is more general than the equation 2-1. Assume that $\vec{p}_i$ is the unit direction vector of the incident ray. $\vec{p}_{i+1}$ is the unit direction vector of the refracted ray. $\vec{u}_i$ is the unit direction vector of the normal, as shown in Figure 2.4. Because $\vec{p}_i$, $\vec{p}_{i+1}$, and $\vec{u}_i$ are in the same plane and satisfy Snell's law, we can have $\vec{u}_i$ as a linear combination of the $\vec{p}_i$ and $\vec{p}_{i+1}$:

$$U_i \, \vec{u}_i = n_{i+1} \, \vec{p}_i - n_i \, \vec{p}_{i+1} \tag{2-2}$$

where $|\vec{u}_i| = |\vec{p}_{i+1}| = |\vec{p}_i| = 1$. Taking the cross product on the both sides of the equation 2-2, and noting that $\vec{u}_i \times \vec{u}_i = 0$, we have:

$$n_{i+1}\,\vec{p}_i \times \vec{u}_i = n_i\,\vec{p}_{i+1} \times \vec{u}_i \Leftrightarrow n_{i+1}\,sin\alpha_{i+1} = n_i\,sin\alpha_i \quad (2\text{-}3)$$

Then, Snell's law in vector form is defined as:

$$\vec{U}_i = n_{i+1}\,\vec{p}_{i+1} - n_i\,\vec{p}_i \quad (2\text{-}4)$$

where $\vec{U}_i = U_i\,\vec{u}_i$.

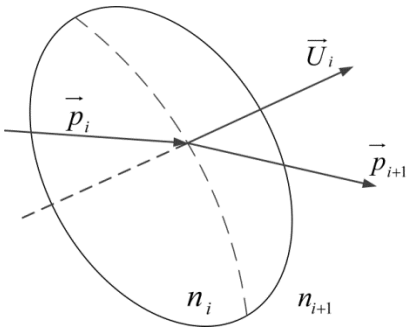

Figure 2.4 Snell's law in vector form

Then, we define the normal of the surface as the composite function of the f_i:

$$\vec{N}_i = \vec{g}(f_i) \quad (2\text{-}5)$$

Now, notice that the normal of the surface and the normal in Snell's law have the same direction. Therefore, we combine the equations 2-4 and 2-5:

$$\frac{\vec{N}_i}{|\vec{N}_i|} = \pm\vec{u}_i = \pm\frac{\vec{U}_i}{U_i} \Leftrightarrow \frac{\vec{g}(f_i)}{|\vec{g}(f_i)|} = \pm\frac{n_{i+1}\,\vec{p}_{i+1} - n_i\,\vec{p}_i}{|n_{i+1}\,\vec{p}_{i+1} - n_i\,\vec{p}_i|} \quad (2\text{-}6)$$

The equation 2-6 is the relation among the input $\vec{p}_i$, the output $\vec{p}_{i+1}$ and the surface f_i for the i th surface. For a lens system which has n surfaces, we have n equations having the form of the equation 2-6. By solving these equations, we can obtain the solution of the lens system.

2.4 Conclusion

An inverse optical design method, Lagrange, is introduced in this chapter. This method eliminates the limitation of the traditional design method by which the initial configurations and the evaluation of the aberration are need. A system of equations can be obtained by connecting the Snell's law in three-dimensional space with the normal of the surface of the lens. The detailed mathematical derivation of the equation of a single surface system is given in the next chapter.

Chapter 3

Single Surface System Design using Lagrange

3.1 Introduction

We define a single surface system as a refractive surface which can perfectly image a single point. This system is composed by a point, a surface and the image without any aberration. The surface separates two mediums with different indices. The whole system is built in spherical coordinates. The Lagrange and fundamental differential geometry is applied to derive the equations in the form of the equation 2-6.

3.2 Spherical Coordinates

The basic properties of the spherical coordinates, (r, θ, φ), are introduced here. The transformation between Cartesian coordinates, (x, y, z), and spherical coordinates is[25]:

$$x = r\ sin\theta\ cos\varphi$$

$$y = r\ sin\theta\ sin\varphi \tag{3-1}$$

$$z = r\ cos\theta$$

A position vector is represented as:

$$\vec{r} = x\ i + y\ j + z\ k \tag{3-2}$$

where the vector i, j and k are unit vectors. They are the Cartesian coordinate basis corresponding to x, y and z axis respectively. The basis of the spherical coordinate is expressed as:

$$\vec{e}_r = \frac{\partial\vec{r}/\partial r}{|\partial\vec{r}/\partial r|} = sin\theta\ cos\varphi\ i + sin\theta\ sin\varphi\ j + cos\theta\ k$$

$$\vec{e}_\theta = \frac{\partial\vec{r}/\partial \theta}{|\partial\vec{r}/\partial \theta|} = cos\theta\ cos\varphi\ i + cos\theta\ sin\varphi\ j - sin\theta\ k \tag{3-3}$$

$$\vec{e}_{\varphi} = \frac{\partial \vec{r}/\partial \varphi}{|\partial \vec{r}/\partial \varphi|} = -sin\varphi\ i + cos\varphi\ j$$

where θ is the angle down from the north pole, and φ is the angle around the equator, as shown in Figure 3.1. We can also use the spherical coordinate basis to express the Cartesian coordinate basis:

$$i = sin\theta\ cos\varphi\ \vec{e}_r + cos\theta\ cos\varphi\ \vec{e}_{\theta} - sin\varphi\ \vec{e}_{\varphi}$$

$$j = sin\theta\ sin\varphi\ \vec{e}_r + cos\theta\ sin\varphi\ \vec{e}_{\theta} + cos\varphi\ \vec{e}_{\varphi} \quad (3\text{-}4)$$

$$k = cos\theta\ \vec{e}_r - sin\theta\ \vec{e}_{\theta}$$

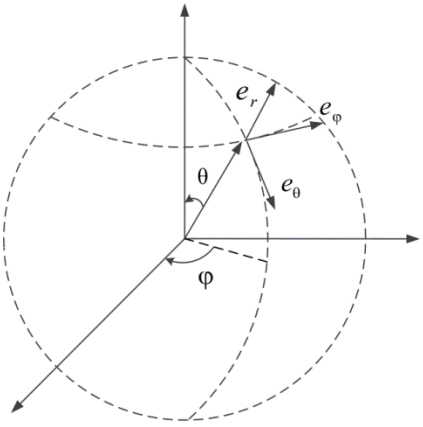

Figure 3.1 Spherical coordinates

Notice that a spherical coordinate is a coordinate system composed by innumerable Cartesian coordinates. Each Cartesian coordinate has the basis corresponding to the specific directions of the position vector, (θ, φ). For example, the Cartesian coordinate corresponding to the direction (θ_1, φ_1) is different from the Cartesian coordinate corresponding to the direction (θ_2, φ_2). These two Cartesian coordinates have different basis.

3.3 The Normal of a Surface in Spherical Coordinates

Figure 3.2 illustrates the definition of the normal of a surface. In spherical coordinates, any surface can be expressed as:

$$\vec{f} = f(\theta, \varphi)\, \vec{e}_r \tag{3-5}$$

where $\vec{f}$ is the position vector for the arbitrary point on the surface. $f(\theta, \varphi)$ is the function of θ and φ. Notice that $\vec{e}_r$ is also the function of θ and φ in terms of the equation 3-3.

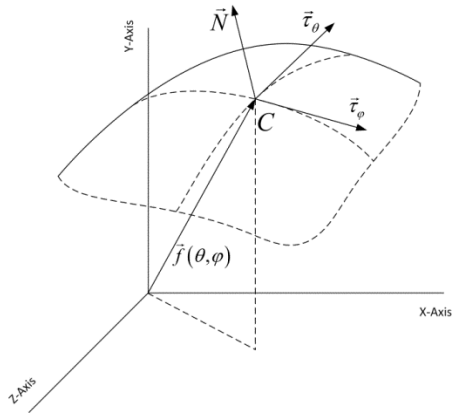

Figure 3.2 The normal of a surface in spherical coordinates

Suppose that there is a point, C, on the surface, and the position vector of C is given by:

$$\vec{f}_c = f(\theta_c, \varphi_c)\, \vec{e}_r(\theta_c, \varphi_c) \tag{3-6}$$

On this surface, we have the θ-parameter curve passing through point C:

$$\vec{\eta}(\theta) = f(\theta, \varphi_c)\, \vec{e}_r(\theta, \varphi_c) \tag{3-7}$$

where φ_c is considered as a constant, and θ is the variable. This curve is shown as the dash line in Figure 3.2. For the same reason, we have the φ-parameter curve:

$$\vec{\psi}(\varphi) = f(\theta_c, \varphi)\ \vec{e}_r(\theta_c, \varphi) \tag{3-8}$$

The tangential vector of the θ-parameter curve is expressed as:

$$\vec{\tau}_\theta(\theta) = \frac{\partial \vec{\eta}(\theta)}{\partial \theta} = \frac{\partial\left(f(\theta,\varphi_c)\ \vec{e}_r(\theta,\varphi_c)\right)}{\partial \theta} = \frac{\partial f(\theta,\varphi_c)}{\partial \theta}\ \vec{e}_r(\theta,\varphi_c) + f(\theta,\varphi_c)\ \vec{e}_\theta(\theta,\varphi_c) \tag{3-9}$$

Then, the tangential vector on point C is given as:

$$\vec{\tau}_\theta(\theta_c) = \frac{\partial f(\theta,\varphi_c)}{\partial \theta}\ \vec{e}_r(\theta,\varphi_c) + f(\theta,\varphi_c)\ \vec{e}_\theta(\theta,\varphi_c)\Big|_{\theta=\theta_c} \tag{3-10}$$

For the same reason, the tangential vector of the φ-parameter curve is expressed as:

$$\vec{\tau}_\varphi(\varphi) = \frac{\partial \vec{\psi}(\varphi)}{\partial \varphi} = \frac{\partial\left(f(\theta_c,\varphi)\ \vec{e}_r(\theta_c,\varphi)\right)}{\partial \varphi} = \frac{\partial f(\theta_c,\varphi)}{\partial \varphi}\ \vec{e}_r(\theta_c,\varphi) + f(\theta_c,\varphi)\ sin\theta_c\ \vec{e}_\varphi(\theta_c,\varphi) \tag{3-11}$$

The tangential vector on point C is:

$$\vec{\tau}_\varphi(\varphi_c) = \frac{\partial f(\theta_c,\varphi)}{\partial \varphi}\ \vec{e}_r(\theta_c,\varphi) + f(\theta_c,\varphi)\ sin\theta_c\ \vec{e}_\varphi(\theta_c,\varphi)\Big|_{\varphi=\varphi_c} \tag{3-12}$$

At last, the normal of the surface at C is defined as:

$$\vec{N} = \vec{\tau}_\theta(\theta_c) \times \vec{\tau}_\varphi(\varphi_c) \tag{3-13}$$

Now, for an arbitrary point on the surface, we define p and q as:

$$p = \frac{\partial f(\theta,\varphi)}{\partial \theta};\ q = \frac{\partial f(\theta,\varphi)}{\partial \varphi} \tag{3-14}$$

According to the equation 3-9, the tangential vector of the θ-parameter curve for the arbitrary point on the surface is:

$$\vec{\tau}_\theta = p\ \vec{e}_r + f\ \vec{e}_\theta \tag{3-15}$$

For the same reason, according to the equation 3-11, the tangential vector of the φ-parameter curve for the arbitrary point is:

$$\vec{\tau}_{\varphi} = q\,\vec{e}_r + f\,sin\theta\,\vec{e}_{\varphi} \tag{3-16}$$

Therefore, for the arbitrary point on the surface, the normal of the surface is expressed as:

$$\vec{N} = \vec{g}(f) = \frac{\partial \vec{f}}{\partial \theta} \times \frac{\partial \vec{f}}{\partial \varphi} = f^2\,sin\theta\,\vec{e}_r - f\,sin\theta\,p\,\vec{e}_{\theta} - f\,q\,\vec{e}_{\varphi} \tag{3-17}$$

3.4 The Differential Equations for the Single Surface System

Now, we start to derive the equations of the system by the Lagrange method. Figure 3.3 is the system layout. Point s is an object on Z axis. s' is the image. $\vec{s}$ represents the position vector of the point s. $\vec{R}_i$ represents an incident ray vector, and $\vec{R}_{i+1}$ represents the refracted ray vector. $\vec{u}_i$ represents the normal direction, which is a unit vector. $\vec{f}_i$ represents the ith surface in a multi-surface system. From the equation 2-2, the direction vector of the normal in Snell's law in three-dimensional space is given as:

$$\vec{u}_i = \frac{\vec{U}_i}{|\vec{U}_i|} \tag{3-18}$$

where $\left|\vec{U}_i\right|$ is equal to U_i which is in the equation 2-2.

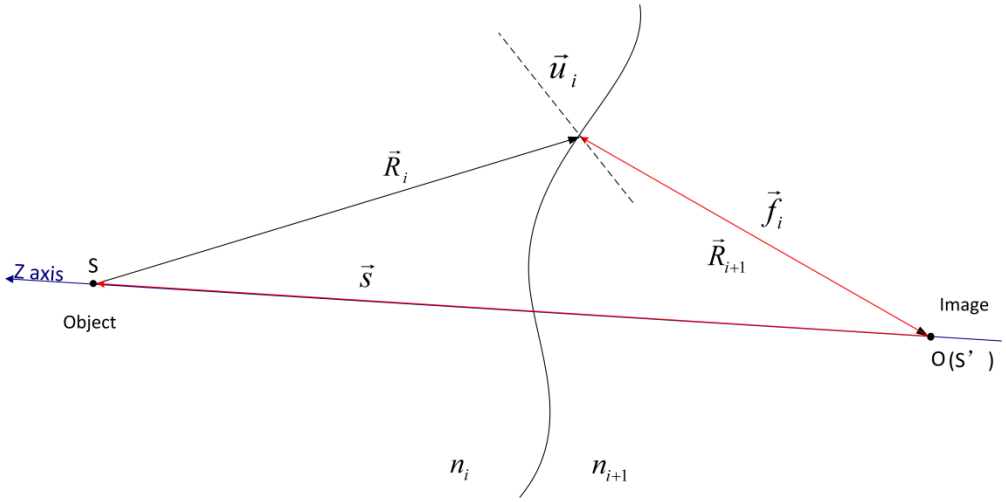

Figure 3.3 The single surface layout

According to the equation 3-17, the normal of the surface is:

$$\vec{N}_i = \vec{g}(f_i) = {f_i}^2 \, sin\theta \, \vec{e}_r - f_i \, sin\theta \, \frac{\partial f_i}{\partial \theta} \, \vec{e}_\theta - f_i \, \frac{\partial f_i}{\partial \varphi} \, \vec{e}_\varphi \tag{3-19}$$

In order to simplify the expressions, we define:

$$p_i = \frac{\partial f_i}{\partial \theta}; q_i = \frac{\partial f_i}{\partial \varphi} \tag{3-20}$$

The magnitude of $\vec{N}_i$ is easy to get as:

$$\left|\vec{N}_i\right| = \sqrt{{f_i}^4 \, sin^2\theta + {f_i}^2 \, sin^2\theta \, p_i^2 + {f_i}^2 \, q_i^2} \tag{3-21}$$

According to the equation 2-6, we have:

$$\vec{u}_i = \frac{\vec{U}_i}{|\vec{U}_i|} = \pm \frac{\vec{N}_i}{|\vec{N}_i|} \tag{3-22}$$

Multiply $\vec{U}_i$ on both sides of the equation 3-22, we have:

$$\left|\vec{U}_i\right| \left|\vec{N}_i\right| = \pm \vec{N}_i \, \vec{U}_i \tag{3-23}$$

Then, substitute the equations 3-19 and 3-21 into 3-23, we have:

$$\left|\vec{U}_i\right| \sqrt{{f_i}^4 \, sin^2\theta + {f_i}^2 \, sin^2\theta \, p_i^2 + {f_i}^2 \, q_i^2} = \pm\left({f_i}^2 \, sin\theta \, U_{i1} - f_i \, sin\theta \, p_i \, U_{i2} - f_i \, q_i \, U_{i3}\right) \tag{3-24}$$

where U_{i1}, U_{i2} and U_{i3} are the three components along the $\vec{e}_r$, $\vec{e}_\theta$ and $\vec{e}_\varphi$ directions respectively. Because the point is on the axis, U_{i3} is equal to 0 (proved by equation 3-40). As a result, the magnitude of $\vec{U}_i$ is:

$$\left|\vec{U}_i\right|^2 = {U_{i1}}^2 + {U_{i2}}^2 \tag{3-25}$$

Then, Square the both sides of the equation 3-24, we have:

$$\left(f_i \, sin\theta \, p_i \, U_{i1} + {f_i}^2 \, sin\theta \, U_{i2}\right)^2 + \left({U_{i1}}^2 + {U_{i2}}^2\right) {f_i}^2 \, q_i^2 = 0 \tag{3-26}$$

This equation is correct if and only if $f_i \, sin\theta \, p_i \, U_{i1} + {f_i}^2 \, sin\theta \, U_{i2} = 0$ and $q_i^2 = 0$. Therefore, we have the differential equations of the single surface system:

$$\begin{cases} p_i \, U_{i1} + U_{i2} \, f_i = 0 \\ q_i = 0 \end{cases} \tag{3-27}$$

3.5 The Solution for Imaging Infinity Object

For the single surface system, i is equal to 1. We suppose that the object s is at infinity. The image s' is at the origin of the coordinates, as shown in Figure 3.3. Then, we have:

$$\vec{s} = (0,0,s_3);\ s_3 \to \infty \tag{3-28}$$

$$\vec{s'} = (0,0,0) \tag{3-29}$$

The surface is expressed as:

$$\vec{f}_1 = f_1\,\vec{e}_r \tag{3-30}$$

where f_1 is the function of θ and φ. Then, the incident ray vector $\vec{R}_1$ is represented as:

$$\vec{R}_1 = \vec{f}_1 - \vec{s} \tag{3-31}$$

We define the magnitude of $\vec{R}_1$ as L_1:

$$L_1 = \left|\vec{R}_1\right| = \sqrt{{f_1}^2 + {s_3}^2 - 2\,\vec{f}_1\,\vec{s}} = \sqrt{{f_1}^2 + {s_3}^2 - 2\,f_1\,s_3\,cos\theta} \tag{3-32}$$

The unit direction vector of the incident ray is defined as $\vec{p}_1$:

$$\vec{p}_1 = \frac{\vec{R}_1}{L_1} \tag{3-33}$$

Then, p_{11}, p_{12} and p_{13} is defined as the three components of $\vec{p}_1$ along the direction of $\vec{e}_r$, $\vec{e}_\theta$ and $\vec{e}_\varphi$ respectively. Therefore,

$$p_{11} = \vec{p}_1\,\vec{e}_r = \frac{\vec{f}_1 - \vec{s}}{L_1}\,\vec{e}_r = \frac{f_1 - s_3\,cos\theta}{\sqrt{{f_1}^2 + {s_3}^2 - 2\,f_1\,s_3\,cos\theta}} \approx -cos\theta$$

$$p_{12} = \vec{p}_1\,\vec{e}_\theta = \frac{\vec{f}_1 - \vec{s}}{L_1}\,\vec{e}_\theta = \frac{s_3\,sin\theta}{\sqrt{{f_1}^2 + {s_3}^2 - 2\,f_1\,s_3\,cos\theta}} \approx sin\theta \tag{3-34}$$

$$p_{13} = \vec{p}_1\,\vec{e}_\varphi = \frac{\vec{f}_1 - \vec{s}}{L_1}\,\vec{e}_\varphi = 0$$

The image is at the origin, so the refracted ray passes through the origin. Therefore, we have:

$$\vec{R}_2 = -\vec{f}_1 \tag{3-35}$$

The magnitude of $\vec{R}_2$ is given by:

$$L_2 = \left|\vec{R}_2\right| = f_1 \tag{3-36}$$

The unit direction vector of the refracted ray is defined as:

$$\vec{p}_2 = \frac{\vec{R}_2}{L_2} = -\vec{e}_r \tag{3-37}$$

Then, the three components of the $\vec{p}_2$ are represented as:

$$p_{21} = -1$$

$$p_{22} = 0 \tag{3-38}$$

$$p_{23} = 0$$

According to Snell's law, the equation 2-2, we have:

$$\vec{U}_1 = n_2\,\vec{p}_2 - n_1\,\vec{p}_1 \tag{3-39}$$

Then, the three components of $\vec{U}_1$ are calculated as:

$$U_{11} = \vec{U}_1\,\vec{e}_r = n_2\,p_{21} - n_1\,p_{11} = -n_2 + n_1\,cos\theta$$

$$U_{12} = \vec{U}_1\,\vec{e}_\theta = n_2\,p_{22} - n_1\,p_{12} = -n_1\,sin\theta \tag{3-40}$$

$$U_{13} = \vec{U}_1\,\vec{e}_\varphi = n_2\,p_{23} - n_1\,p_{13} = 0$$

At last, substituting the equation 3-40 into the differential equations 3-27, we have the equations of the single surface system:

$$\begin{cases} (-n_2 + n_1\,cos\theta)\,\frac{\partial f_1}{\partial \theta} - n_1\,sin\theta\,f_1 = 0 \\ \frac{\partial f_1}{\partial \varphi} = 0 \end{cases} \tag{3-41}$$

Because of $\frac{\partial f_1}{\partial \varphi} = 0$, the equations are transformed into a first order ordinary differential equation under the initial condition, $f_1(0) = r_1$, which is:

$$(-n_2 + n_1\, cos\theta)\, \frac{\partial f_1}{\partial \theta} - n_1\, sin\theta\, f_1 = 0;\; f_1(0) = r_1 \tag{3-42}$$

This equation can be easily solved by software on computer, MATLAB or Wolfram Mathematica. The solution is given by:

$$f_1(\theta) = \frac{(n_1 - n_2)\, r_1}{-n_2 + n_1\, cos\theta} \tag{3-43}$$

At last, the surface solution in Spherical coordinates is expressed as:

$$\vec{f_1} = \frac{(n_1 - n_2)\, r_1}{-n_2 + n_1\, cos\theta}\, \vec{e}_r \tag{3-44}$$

3.6 Conclusion

The differential equations of a single surface image system are built in spherical coordinates. This system can perfectly image a point on the optical axis. For the point at infinity, a first order ordinary differential equation is derived, and the expression of the surface is obtained by solving the equation. Based on this solution, two lens design examples are introduced in the next chapter. These two lenses are designed as aberration free systems.

Chapter 4
Lens Design Examples

4.1 Introduction

In order to assess the single surface solution obtained in the previous chapter, we provide two types of the lens design examples, a Plano-convex lens and a Bi-convex lens. The optical design software, ZEMAX, was used to simulate the lenses and evaluate their image qualities. ZEMAX produced by Radiant Zemax Ltd. can be used to visualize and analyze optical systems by ray tracing. We use ZEMAX to evaluate whether our systems are aberration free or not.

4.2 A Plano-convex Lens Example

We want to design a Plano-convex lens whose back focal length is 30 millimeter (mm). The lens can image an on-axis point at infinity without any aberration. The front surface of the lens is a plane surface, and the back surface is the solution from the Lagrange equations. The index of the lens is 1.53, and the diameter of the lens is 16mm; therefore, the field of view of the lens is 30 degree. The field of view of a lens is defined as α:

$$\alpha = 2arctan\frac{d}{2f} \tag{4-1}$$

where d is the diameter of the exit aperture of the lens, and f is the back focal length. The incident rays are parallel to the axis because the object is at infinity. Therefore, the lens is same as the single surface system which has already been discussed in the previous chapter. The solution of the back surface is:

$$f_1(\theta) = \frac{(n_1 - n_2)\, r_1}{-n_2 + n_1\, cos\theta}\ \vec{e}_r \tag{4-2}$$

where $n_1 = 1.53$, $n_2 = 1$ and $r_1 = 30$. The r_1 is assigned to 30 mm here because the back focal length of the Plano-convex lens is 30 mm. In order to simulate the surface solution in ZEMAX, the exact solution 4-2 has to be fitted to the aspherical surface polynomial. In ZEMAX, we chose the surface type as extended even asphere surface to fit our solution, the equation 4-2. As a result, an approximation is needed.

In ZEMAX, each surface has its own Cartesian coordinate. The optical axis of an optical system is defined as the rotational symmetry axis. The surface vertex is the origin of the coordinate. Both the x and y axis pass through the vertex and vertical to the optical axis. The aspherical surface polynomial in ZEMAX is defined as:

$$z(r) = \frac{c\,r^2}{1+\sqrt{1-(1+k)c^2\,r^2}} + \alpha_4\,r^4 + \alpha_6\,r^6 + \alpha_8 r^8 + \cdots \tag{4-3}$$

where the $z(r)$ represents the sag (height) of the surface. r represents the radial distance from the optical axis. c represents the vertex curvature, and k is the conic constant. In this example, we assume that k is equal to zero.

Now, the form of the equation 4-2 need to be transferred from spherical coordinates to Cartesian coordinate. In terms of the equation 3-1 and 3-1, the transformation result can be obtained as:

$$z'(r) = -\left(\frac{{n_1}^2\,r_1 - n_1\,n_2\,r_1 + \sqrt{{n_1}^2\,{n_2}^2\,r^2 - {n_2}^4\,r^2 + {n_1}^2\,{n_2}^2\,{r_1}^2 - 2n_1\,{n_2}^3\,{r_1}^2 + {n_2}^4\,{r_1}^2}}{{n_1}^2 - {n_2}^2} - r_1\right) \tag{4-4}$$

Substituting $n_1 = 1.53$, $n_2 = 1$ and $r_1 = 30$ into the equation 4-4, we have:

$$z'(r) = 30 - 0.745767769(24.327 + \sqrt{252.81 + 1.3409r^2}) \tag{4-5}$$

Then, we are looking for the curvature c and the coefficients α_i $(i = 4,6,\cdots)$ in the equation 4-3. To find the coefficients, we expand both $z(r)$ and $z'(r)$ into Taylor series. The curvature and coefficients can be obtained by comparing the coefficients in these two Taylor series. The equation 4-4 and 4-5 are expanded at $r = 0$:

$$z(r) = \frac{c\,r^2}{2} + \left(\alpha_4 + \frac{c^3}{8}\right)r^4 + \left(\alpha_6 + \frac{c^5}{16}\right)r^6 + \left(\alpha_8 + \frac{5c^7}{128}\right)r^8 + \cdots + \left(\alpha_{30} + \frac{334305\,c^{29}}{67108864}\right)r^{30} + O[r]^{31} \tag{4-6}$$

$$z'(r) = \alpha'_2\,r^2 + \alpha'_4\,r^4 + \alpha'_6\,r^6 + \alpha'_8\,r^8 + \cdots + \alpha'_{30}\,r^{30} + O[r]^{31} \tag{4-7}$$

The values of the coefficients in the equation 4-7 are listed in Table 4.1.

Table 4.1 The values of the coefficients in the equation 4-7 for the Plano-convex lens

$\alpha'_2 = -0.03144654088050315$	$\alpha'_4 = 0.00004169798135622274$
$\alpha'_6 = -1.105826968880959 \times 10^{-7}$	$\alpha'_8 = 3.665804810362721 \times 10^{-10}$
$\alpha'_{10} = -1.361035706321253 \times 10^{-12}$	$\alpha'_{12} = 5.414182919799957 \times 10^{-15}$
$\alpha'_{14} = -2.256314924498844 \times 10^{-17}$	$\alpha'_{16} = 9.723558420697984 \times 10^{-20}$
$\alpha'_{18} = -4.297799232069514 \times 10^{-22}$	$\alpha'_{20} = 1.937613678944548 \times 10^{-24}$
$\alpha'_{22} = -8.87565175784872 \times 10^{-27}$	$\alpha'_{24} = 4.119176955752118 \times 10^{-29}$
$\alpha'_{26} = -1.932711716297499 \times 10^{-31}$	$\alpha'_{28} = 9.152741543562206 \times 10^{-34}$
$\alpha'_{30} = -4.369138887775922 \times 10^{-36}$	

By comparing the coefficients of the equation 4-6 and 4-7, we can find the relation between α_i and α'_i $(i = 4, 6, 8 \cdots 30)$, as shown in Table 4.2:

Table 4.2 The coefficient relation between the equations 4-6 and 4-7

$c = 2\,\alpha'_2$	$\alpha_4 = \alpha'_4 - \frac{c^3}{8}$
$\alpha_6 = \alpha'_6 - \frac{c^5}{16}$	$\alpha_8 = \alpha'_8 - \frac{5c^7}{128}$
$\alpha_{10} = \alpha'_{10} - \frac{7c^9}{256}$	$\alpha_{12} = \alpha'_{12} - \frac{21c^{11}}{1024}$
$\alpha_{14} = \alpha'_{14} - \frac{33c^{13}}{2048}$	$\alpha_{16} = \alpha'_{16} - \frac{429c^{15}}{32768}$
$\alpha_{18} = \alpha'_{18} - \frac{715c^{17}}{65536}$	$\alpha_{20} = \alpha'_{20} - \frac{2431c^{19}}{262144}$
$\alpha_{22} = \alpha'_{22} - \frac{4199c^{21}}{524288}$	$\alpha_{24} = \alpha'_{24} - \frac{29393c^{23}}{4194304}$
$\alpha_{26} = \alpha'_{26} - \frac{52003c^{25}}{8388608}$	$\alpha_{28} = \alpha'_{28} - \frac{185725c^{27}}{33554432}$
$\alpha_{30} = \alpha'_{30} - \frac{334305\,c^{29}}{67108864}$	

Then, α'_i can be calculated according to Table 4.1 and 4.2. The α'_i values are given in Table 4.3:

Table 4.3 The values of the coefficients ready for simulation for the Plano-convex lens

$c = -0.0628930817610063$	
$\alpha_4 = 0.00007279499183890061$	$\alpha_6 = -4.907996661105414 \times 10^{-8}$
$\alpha_8 = 5.186282893632812 \times 10^{-10}$	$\alpha_{10} = -9.400339032719032 \times 10^{-13}$
$\alpha_{12} = 6.663149939644952 \times 10^{-15}$	$\alpha_{14} = -1.497754744437778 \times 10^{-17}$
$\alpha_{16} = 1.097108696803296 \times 10^{-19}$	$\alpha_{18} = -3.886578503942006 \times 10^{-22}$
$\alpha_{20} = 2.075874672935443 \times 10^{-24}$	$\alpha_{22} = -8.403331746444717 \times 10^{-27}$
$\alpha_{24} = 4.28265150580097 \times 10^{-29}$	$\alpha_{26} = -1.875509824771732 \times 10^{-31}$
$\alpha_{28} = 9.35476328887972 \times 10^{-34}$	$\alpha_{30} = -4.297219434120701 \times 10^{-36}$

Finally, we need to evaluate the approximate error. Because $z(r)$ and $z'(r)$ are expanded at $r = 0$. Therefore, the largest error occurs when r is maximum. The maximum r is equal to 8 because the aperture size of the lens is 8 mm. The error is given as:

$$z(r_{max}) = z'(r_{max}) + error_{max} \tag{4-8}$$

$$error_{max} = |z(r_{max}) - z'(r_{max})| = |z(8) - z'(8)| = 0.00001628865824 \tag{4-9}$$

The error is small enough to be neglected.

Now, we are ready to simulate the lens in ZEMAX. The steps for the simulation are illustrated in Figure 4.1.

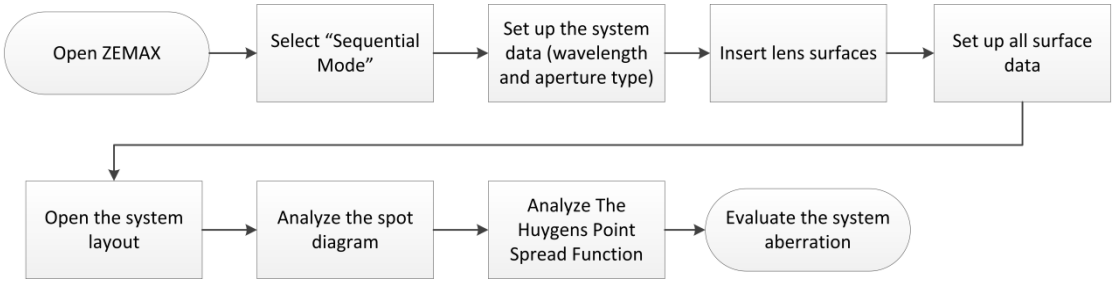

Figure 4.1 The simulation steps in ZEMAX

First, we open ZEMAX, and set it into "Sequential Mode". The "Sequential Mode" and "Non-sequential Model" can be chosen in "File" menu. Keep "field data" and "wavelength data" as default. We only use one field in object space , and the field angle is zero. The wavelength is 0.55 microns as default. Click the "Gen" button on the shortcut bar to open the "General" window. In this window, in order to prevent the marginal rays being blocked by the aperture, we need to change "Aperture Type" to "Entrance Pupil Diameter", and change the "Aperture value" to 16, which is same as the diameter of the lens, 16 mm.

Second, we set up the surfaces in "Lens Data Editor" window. Insert two surfaces after "OBJ" which is the object surface of the system. Then, we set the surface data:

Surface "OBJ":

Surf: Type Standard

Comment OBJECT

Radius Infinity

Thickness Infinity

Surface “1”:

Surf: Type Standard

Comment REFERENCE SURFACE

Radius Infinity

Thickness 20

Notice: this surface is just for clearly illustrating the layout of the lens. We call it dummy surface.

Surface “2”:

Surf: Type Standard

Comment FRONT SURFACE

Radius Infinity

Thickness 4

Glass Model; 1.53 0.0

Semi-Diameter 8

Surface “STO”:

Surf: Type	Ext Asphere
Comment	BACK SURFACE
Radius	-15.9
Thickness	Solve Type: Marginal Ray Height
	Height: 0
	Pupil Zone: 0
Semi-Diameter	8

Notice: The surface “STO” represents the stop or aperture. The radius of this surface can be calculated by taking the reciprocal of the curvature c, which is given in Table 4.3. The Marginal Ray Height Solve (M-Solve) is the solve type to find the paraxial back image distance[26].

Open “Extra Data Editor” window in “Editor” menu. In this window, we set the “Max Term#” of “STO*” surface to 15 and “Norm Radius” to 1. Then, input all the polynomial coefficients which are given in Table 4.3.

Now, we can check the layout of the system by clicking the “Lay” button on the shortcut bar. The layout is shown in Figure 4.2. Only the chief ray and marginal rays are displayed here. Of cause, you can change the number of rays displayed in the “setting” tab.

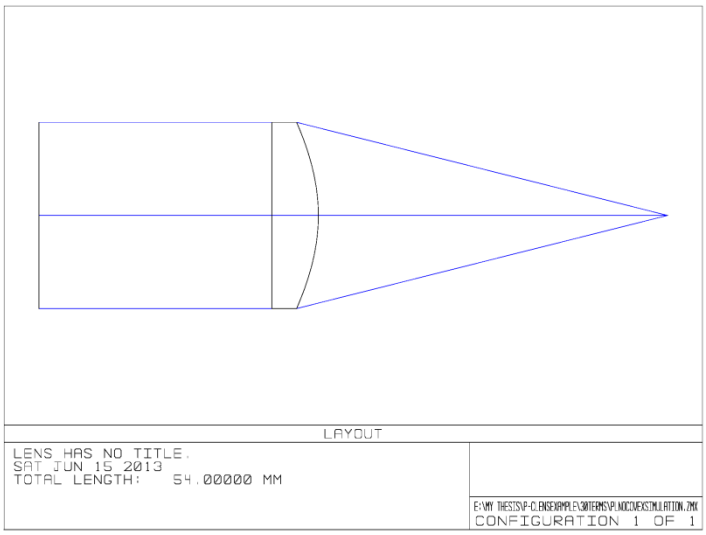

Figure 4.2 The layout of the Plano-convex lens in ZEMAX

The spot diagram can be found in analysis menu. It is shown as Figure 4.3.

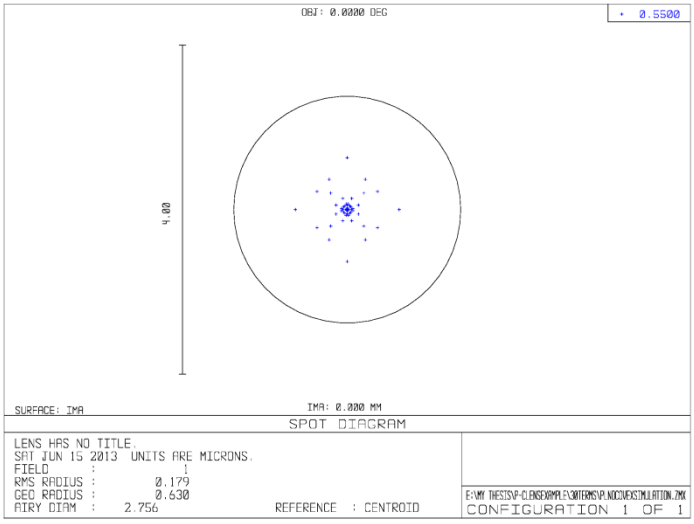

Figure 4.3 The spot diagram of the Plano-convex lens in ZEMAX

In Figure 4.3, the circle is the airy disk of the system. The radius of the airy disk is 1.22 times wavelength[27]. In Figure 4.3, we can see that the RMS radius of the spots is 0.179 microns. This

value is much smaller than the radius of the airy disk, 2.756 microns. It is also found that all the spot are inside the airy disk. Therefore, the optical system is diffraction limited.

The Huygens Point Spread Function can also be checked in the analysis menu, as shown in Figure 4.4.

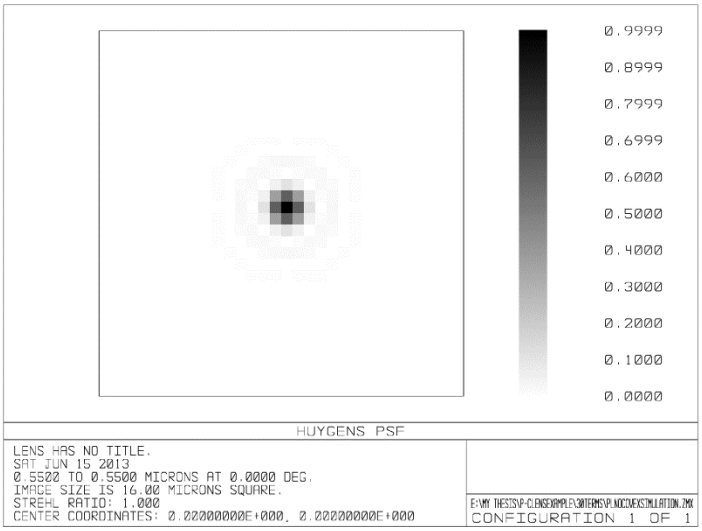

Figure 4.4 The Huygens Point Spread Function of the Plano-convex lens in ZEMAX

This figure illustrates that the Strehl Ratio of the system is 1. Strehl ratio refers to the ratio of the peak intensity of the point spread function (PSF) with aberrations to the peak intensity of the PSF without aberration. The unit Strehl Ratio means the lens is already aberration free[27].

4.3 A Bi-convex Lens Example

We want to perfectly image the object not only at infinity but also at the mid-distant and near-distant. A Bi-convex lens can be designed to image near object. For example, we need image a point on-axis which is 1 meter from the vertex of the front surface of a Bi-convex lens; and the image is 30 mm away from the back surface vertex on axis.

The design idea is described as following: first, according to the reversibility of the ray in geometric optics, one point can be imaged to infinity by the Plano-convex lens given in previous section; then, we use another Plano-convex lens to image this infinity image on the designed point; at last, we combine these two Plano-convex lenses to obtain the Bi-convex lens.

We start at designing the first half of the Bi-convex lens. The previous solution, the equation 3-44, is again used. This time, set n_1 to 1.5, n_2 to 1 and r_1 to 1000 mm (1 meter). By the same way as the pervious example, we have the transformed solution as:

$$-z'(r) = -1000 + 0.745767768(810.9 + \sqrt{280900. + 1.3409r^2}) \quad (4\text{-}10)$$

The negative sign means that the surface is inversed. The polynomial coefficients can also be obtained by the same method as previous example. The results are shown in Table 4.4.

Table 4.4 The values of the coefficients for the front surface of the Bi-convex lens

$c = 0.001886792452830189$	
$\alpha_4 = -1.965464779650315 \times 10^{-9}$	$\alpha_6 = 1.192643188648614 \times 10^{-15}$
$\alpha_8 = -1.134240068837495 \times 10^{-20}$	$\alpha_{10} = 1.850268731810085 \times 10^{-26}$
$\alpha_{12} = -1.180357022358282 \times 10^{-31}$	$\alpha_{14} = 2.387904837416268 \times 10^{-37}$
$\alpha_{16} = -1.574231065932167 \times 10^{-42}$	$\alpha_{18} = 5.019133815113658 \times 10^{-48}$
$\alpha_{20} = -2.412709142674087 \times 10^{-53}$	$\alpha_{22} = 8.790181814979436 \times 10^{-59}$
$\alpha_{24} = -4.031824265643405 \times 10^{-64}$	$\alpha_{26} = 1.589098111427521 \times 10^{-69}$
$\alpha_{28} = -7.13356594083297 \times 10^{-75}$	$\alpha_{30} = 2.949197913834118 \times 10^{-80}$
$error_{max} = \lvert z(8) - z'(8) \rvert = 1.89654 \times 10^{-13}$	

Again, the approximate error is so small that it can be neglected.

We continue building the Bi-convex lens on the previous Plano-convex lens, which, now, is the back half of the Bi-convex lens. We change the “Surf: Type” of the surface 2 from “Standard” to “Ext Asphere”. This surface represents the front surface. Keep other surfaces data same as the previous example. The setting for surface 2 is given as:

Surface “2”:

Surf: Type	Ext Asphere
Comment	FRONT SURFACE
Radius	530
Thickness	3
Glass	Model; 1.53 0.0
Semi-Diameter	Solve Type: Automatic

Open the “General” window from the shortcut tools, and change the “Aperture Type” to “Entrance Pupil Diameter”, and set the “Aperture Value” to 16. Then, open the “Extra Data Editor” window. Set the “Max Term#” to 15 and the “Norm Radius” to 1 for the surface 2. At last, input all the polynomial coefficients in Table 4.4 into the “Extra Data Editor” window. The layout is shown in Figure 4.5; the spot diagram is given in Figure 4.6; and the Huygens Point Spread Function is also illustrated in Figure 4.7.

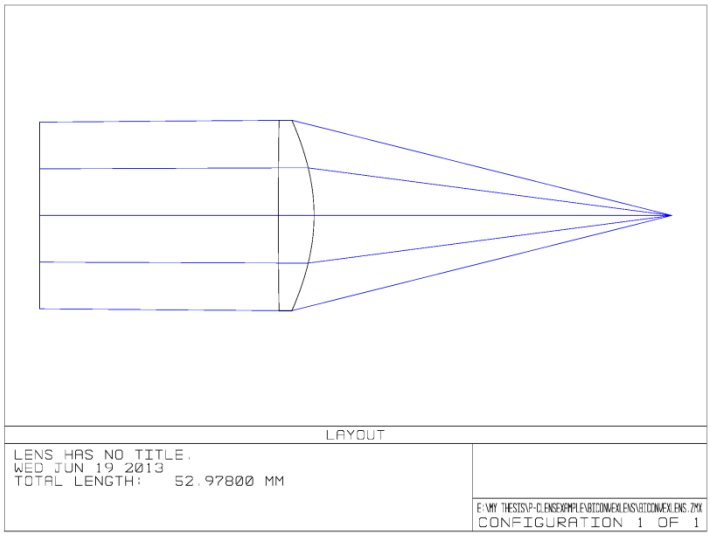

Figure 4.5 The layout of the Bi-convex lens in ZEMAX

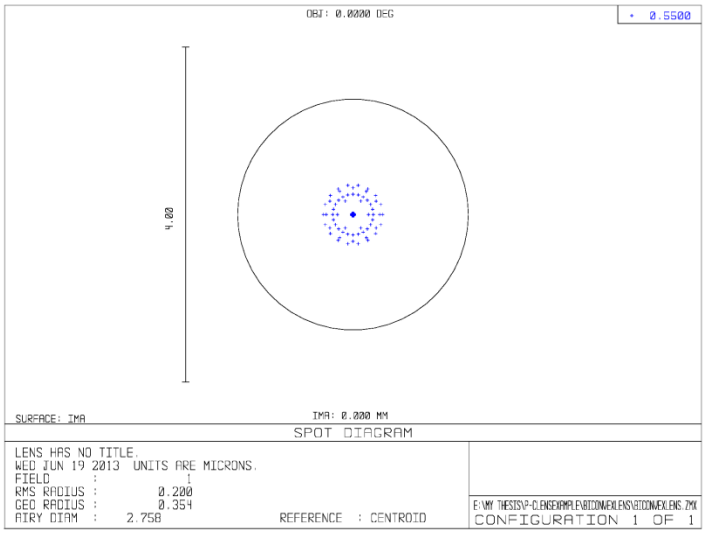

Figure 4.6 The spot diagram of the Bi-convex lens in ZEMAX

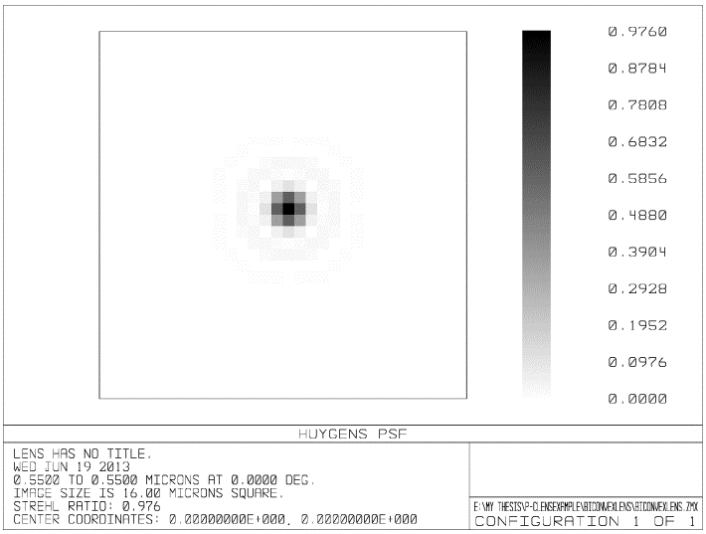

Figure 4.7 The Huygens Point Spread Function of the Bi-convex lens in ZEMAX

Again, in Figure 4.6, we can find that the RMS radius, which is 0.2 micros, is much smaller than the radius of the airy disk, 2.758 micros. In Figure 4.7, the Strehl Ratio is 0.976, which means that the lens is an aberration free system.

4.4 Conclusion

The Plano-convex lens and Bi-convex lens for imaging distant and near point are designed in terms of the solution obtained in chapter 3. The Bi-convex lens is just a combination of two Plano-convex lenses. Both of the two lenses are aberration free. This is proved by analyzing the spot diagrams and Point Spread Function of the lenses in Zemax.

Chapter 5
Conclusion

The objective of the study was to introduce a new spectacle lens design technique, the Lagrange, which is different from traditional lens design methods. It is an inverse, analytic and three-dimensional design technique, which helps in designing personalized spectacle lens. Comparing with traditional methods, the Lagrange solves unknown lens surface based on definable inputs and outputs (objects and images) according to customer requirements. This increases the degree of freedom and the flexibility of the design. The method is efficient for the spectacle lens which has limited surfaces. Moreover, in this method, the definable outputs make the simultaneous elimination of several aberrations possible.

5.1 The Lagrange Method Conclusion

The Lagrange is to solve an unknown optical system by the given input and output ray fields, which are unified vector functions with the system parameters as variables in terms of the object and image of the system. In order to build the mathematic model of the lens systems in three-dimensional space, the Snell's law is generalized to a vector form and combined with the surface normal in fundamental differential geometry. For a single aberration free surface to image a point at infinity, the Lagrange derives a system of partial differential equations, and the solution is an exact expression.

In spherical coordinates, the differential equations of a single aberration free surface for imaging a single point is:

$$\begin{cases} p_i\, U_{i1} + U_{i2}\, f_i = 0 \\ q_i = 0 \end{cases} \tag{5-1}$$

where f_i represents the ith surface in a multi-surface system; $p_i = \frac{\partial f_i}{\partial \theta}$; $q_i = \frac{\partial f_i}{\partial \varphi}$ and U_{i1}, U_{i2} and U_{i3} are the three components of the normal of the surface along the $\vec{e}_r$, $\vec{e}_\theta$ and $\vec{e}_\varphi$ directions respectively.

The differential equations of a single aberration free surface for imaging a single point at infinity are:

$$\begin{cases} (-n_2 + n_1\, cos\theta)\, \frac{\partial f}{\partial \theta} - n_1\, sin\theta\, f = 0 \\ \frac{\partial f}{\partial \varphi} = 0 \end{cases} ; f(0) = r \tag{5-2}$$

where r is the distance from the vertex point of the surface to the image point. The solution of the equations is:

$$\vec{f} = \frac{(n_1 - n_2)\, r}{-n_2 + n_1\, cos\theta}\, \vec{e}_r \tag{5-3}$$

Based on this solution, two lens design examples were obtained to evaluate the Lagrange method. First, a Plano-Convex lens was design to image an on-axis point at infinity. The front surface of the lens was a plane surface, and the back surface used the equation 5-3. Second, a Bi-Convex lens can be designed to image near object. The Bi-Convex lens was just a combination of two Plano-Convex lenses. In terms of the image analysis in ZEMAX, we found that these two lenses were aberration free. As a result, the solution from the Lagrange fitted our requirement of designing an aberration free system.

5.2 Discussion and Future Work

Traditional spectacle lens design is based on the two-dimensional (2D) ray tracing and aberration theory, which consider the lens system is rotational symmetric around an optical axis. This design method is a forward and numerical method, as explained in chapter 2, which is widely applied on finished lenses. The defects of the traditional lenses are obvious. First, the optical axis of the lens is also its rotational symmetry axis, and Snell's law is approximately linear only in the paraxial area of the lens. As a result, only the center of the lens is well designed, and the image quality becomes worse towards the lens periphery. Second, the finished lenses have the limitations for the spectacle lens application because of the flexibility of the individual's eye data. The human eye is a

complicated optical system, and the eye parameters vary with individuals. Moreover, the finished lenses do not always meet the various visual behavior requirements.

Modern spectacle lenses tend to focus on semi-finished lenses or customized lenses which have two free-form surfaces. This personalized lens can combine individual's eye parameters and their visual demands. Future work will focus on further application of the Lagrange for the personalized lens design. The Lagrange will be used to design the unfinished surface of the semi-finished lens according to the unique prescription of each patient. When the patient gazes through the lens periphery, the aberrations including oblique astigmatism, field of curvature, distortion and even spherical aberration will be eliminated. This means that the lens will have more than one optical axis in terms of the number of the gazing directions. In conclusion, a multi-axis surface designed by the Lagrange will be the objective in future.

References

[1] D. A. Atchison, “Modern Optical Design Assessment and Spectacle Lenses,” *Opt. Acta Int. J. Opt.*, vol. 32, no. 5, pp. 607–634, May 1985.

[2] J. Chaves, *Introduction to nonimaging optics*. New York: CRC Press, 2008, p. 5.

[3] E. Hecht, *Optics*, Fourth edi. MA: Addison-Wesley Publishing Company, 2001, p. 253.

[4] W. J. Smith, *Modern optical engineering: the design of optical systems*, Third edit. New York: McGraw-Hill Professional, 2000, p. 63.

[5] W. J. Smith, *Modern optical engineering: the design of optical systems*, Third edit. New York: McGraw-Hill Professional, 2000, p. 64.

[6] M. Jalie, *The Principles of Ophthalmic Lenses*, Fourth edi. London: The association of dispensing opticians, 1984, p. 390.

[7] R. Kingslake and R. B. Johnson, *Lens Design Fundamentals*, Second edi. New York: Academic Press, 2009, pp. 289–294.

[8] D. Atchison, “Third-order theory of spectacle lenses applied to correction of peripheral refractive errors,” *Optom. Vis. Sci.*, vol. 88, no. 2, pp. E227–E233, 2011.

[9] M. Jalie, *The principles of ophthalmic lenses*, Fourth edi. London: The association of dispensing opticians, 1984, pp. 404–406.

[10] D. Atchison and G. Smith, “Spectacle Lenses and Third-order Distortion,” *Ophthalmic Physiol. Opt.*, vol. 7, no. 3, pp. 303–308, 1987.

[11] D. J. Meister and S. W. Fisher, “Progress in the spectacle correction of presbyopia. Part 1: Design and development of progressive lenses.,” *Clin. Exp. Optom.*, vol. 91, no. 3, pp. 240–50, May 2008.

[12] J. SHEEDY and C. Campbell, “Progressive powered lenses: the Minkwitz theorem,” *Optom. Vis. Sci.*, vol. 82, no. 10, pp. 916–922, 2005.

[13] J. Winthrop, “Progressive power ophthalmic lens having a plurality of viewing zone with discontinuous power variations therebetween,” *US Pat. 4,062,629*, 1977.

[14] D. Meister and J. Sheedy, *Introduction to Ophthalmic Optics*, Seventh ed. Carl Zeiss Vision, 2010, p. 75.

[15] G. Smith and D. A. Atchison, “Effect of conicoid asphericity on the Tscherning ellipses of ophthalmic spectacle lenses,” *J. Opt. Soc. Am.*, vol. 73, no. 4, p. 441, Apr. 1983.

[16] J. Schwiegerling, *Field Guide To Visual And Ophthalmic Optics*. Bellingham,WA: SPIE Press, 2004, p. 26.

[17] D. A. Atchison, "Third-order Theory and Aspheric Spectacle Lens Design," *Ophthalmic Physiol. Opt.*, vol. 4, no. 2, pp. 179–186, Apr. 1984.

[18] S. Barbero, "Minimum tangential error ophthalmic lens design without multi-parametric optimization," *Opt. Commun.*, vol. 285, no. 12, pp. 2769–2773, Jun. 2012.

[19] D. A. Atchison, "Spectacle lens design: a review," *Appl. Opt.*, vol. 31, no. 19, pp. 3579–85, Jul. 1992.

[20] D. A. ATCHISON, "Spectacle Lens Design - Development and Present State," *Clin. Exp. Optom.*, vol. 67, no. 3, pp. 97–107, May 1984.

[21] D. Meister and J. Sheedy, *Introduction to Ophthalmic Optics*, Seventh ed. Carl Zeiss Vision, 2010, p. 7.

[22] L. Kong and C. Cheung, "An Integrated Manufacturing System for the Design, Fabrication, and Measurement of Ultra-Precision Freeform Optics," *Electron. Packag. Manuf. IEEE Trans.*, vol. 33, no. 4, pp. 244 – 254, 2010.

[23] M. Schinhaerl, R. Stamp, E. Pitschke, R. Rascher, L. Smith, G. Smith, A. Geiss, and P. Sperber, "Advanced techniques for computer-controlled polishing," in *SPIE 7060, Current Developments in Lens Design and Optical Engineering IX*, 2008, p. 70600Q.

[24] M. D. Tocci, "How to Modelthe Human Eye in Zemax," 2007. [Online]. Available: http://contrast.zbytesoftware.net/wp/wp-content/uploads/2013/05/CODE_Eye_article.pdf.

[25] G. B. Arfken, H. J. Weber, and F. E. Harris, *Mathematical Methods for Physicists International Sixth Edition*. Elsevier Academic Press, 2005, pp. 123–126.

[26] J. Geary, *Introduction to Lens Design With Practical ZEMAX® Examples*. Verginia, USA: Willmann-Bell,Inc, 2002, p. 85.

[27] R. ZEMAX, "Optical Design Program–User's Manual," 2012.